EFFECTS OF INLET TURBULENCE INTENSITY AND INLET SWIRL ON DIFFUSER FLOWS

H. A. Abdalla, M. M. El-Mayit**,*
*B. A. Khalifa***, and A. M. El-Shazly*****
Department of Mechanical Power Engineering,
Faculty of Engineering, Menoufia University,
Shebin El-Kom, Egypt.

* Assistant Professor, ** Lecturer, *** Professor, **** Graduate Student

ABSTRACT

The numerical prediction of the turbulent flow filed in the conical diffusers with the k-ε model of turbulence is presented. The numerical calculation is based on the fully conservative control volume representation of governing conservation equations. Complex turbulent flows inside various conical diffusers with the effects of inlet turbulence intensity and inlet swirl have been numerically predicted. The numerical prediction compares generally well with the experiments. The results show that, increasing the inlet turbulence intensity has resulted in a significant improvement of the diffuser performance. However, an optimum inlet turbulence intensity for improving the static pressure recovery of the diffuser is observed.

The effect of swirling inlet flow on diffuser performance was found to be a strong function of the flow regime in the same diffuser with axial flow. Swirling inlet flow slightly affect the performance of non-separated diffuser flow while swirling inlet flow caused a large improvement for wide-angled diffusers based on inlet swirl intensity. Optima of swirl intensity are presented for the various swirl angles investigated. It is also found that, the decay of swirl is strongly affected by the flow regimes in conical diffusers.

1- INTRODUCTION

Flow in a diffuser is of considerable practical importance in wind tunnels, air breathing propulsion systems and in turbomachines. In contrast, flow at the

MANUSCRIPT RECEIVED FROM DR: H. A. ABDALLA AT:27/2/1996,
ACCEPTED AT:24/3/1996, PP 49 - 71
ENGINEERING RESEARCH BULLETIN,VOL,19,NO. 2, 1996
MENOUFIYA UNIVERSITY, FACULTY OF ENGINEERING,
SHEBINE EL-KOM, EGYPT. ISSN. 1110 - 1180

inlet of the diffuser such as exists in a gas turbine or air breathing system is distorted by wall boundary layers and blade wakes. In addition, the swirling inlet velocity component in the diffuser is often observed in flow downstream of the gas turbine or certain types of combustor chambers. Consequently, the overall performance of such turbomachines is strongly influenced by the exit conditions of the diffuser. This may result in an increase of aerodynamic losses due to the non-uniformity of velocity profile at diffuser exit.

A classification of flow regimes and the effect of inlet conditions on the performance of plane and conical diffusers can be found in Ref.[1] to Ref. [6]. They clearly demonstrated the importance of inlet conditions on the mean flow development, especially for diffusing ducts. It was found that boundary layer blockage, inlet distortion and swirl have a marked effect on diffuser performance. The effect of inlet distortion on conical diffuser were experimentally studied by Sajben et.al. [7], Sharan [8], while the effect of inlet swirl was studied experimentally by McDonald et. al. [9], Senoo et. al. [10] and Neve and Wirasinghe [11]. Recently, Steven, et. al.[12] predicted the turbulence quantities by k-ε model and algebraic Reynolds stress turbulence model for swirling flow through 12 and 20 degrees conical diffusers. Measurements of the swirling boundary layer developing in the 20 degrees conical diffuser were made by Clausen et. al. [13]. The inlet swirl was close to solid-body rotation and was of sufficient magnitude to prevent boundary layer separation but just insufficient to cause recirculation in the core flow. All six Reynolds stresses were measured within the boundary layer using a hot wire. The results indicated that certain types of inlet distortion increase diffuser pressure recovery coefficients. On the other hand, with the swirling velocity component, the flow is pressed towards the wall by the centrifugal force and the wall boundary layer is less likely to separate even if the divergence angle of the diffuser is large, and a high pressure recovery coefficient is observed. However, large amount of swirl reduces the axial velocity too far near the centerline of the diffuser or induces a reversed flow region, which results in a low-pressure recovery rate.

With long approach pipes, diffuser performance rises as approach lengths increase. This was attributed to changes in turbulence level which enhances mixing transverse to the flow direction, thus reducing distortions. Hence, turbulence is indeed an additional inlet parameter affecting diffuser flow. Moore and Kline [14], Sajben et. al. [15] and Hoffmann [16] altered inlet velocity and turbulence characteristics to improve the overall diffuser efficiency. It appeared from the previous studies that, with the inlet flow control device such as rod or vortex generator, the high energy fluid outside the wall boundary layer of the diffuser is mixed with the flow energy fluid inside the boundary layer to delay the separation and to maintain large effective area. The possibility of predicting these flows with the effects of inlet swirl and inlet distortion has not been previously studied in details and this is the subject of the present study.

2- MATHEMATICAL MODEL

2.1 Governing Equations and Turbulence Closure

The cylindrical coordinate-system is used to describe the flow in the axisymmetric conical diffuser, Fig.(1). For the present study, the steady state equations for incompressible, axisymmetric, turbulent swirling flow may be written in general form as follows [17],

$$\frac{1}{r}\left[\frac{\partial}{\partial x}(\rho u r \phi)+\frac{\partial}{\partial r}(\rho v r \phi)-\frac{\partial}{\partial x}(r \Gamma_\phi \frac{\partial \phi}{\partial x})-\frac{\partial}{\partial r}(r \Gamma_\phi \frac{\partial \phi}{\partial r})\right]=S_\phi \qquad (1)$$

The fluxes for the source term S_ϕ are given in table (1), where certain quantities are defined as follows:

$$S^u=\frac{\partial}{\partial x}(\mu \frac{\partial u}{\partial x})+\frac{1}{r}\frac{\partial}{\partial r}(r \mu \frac{\partial v}{\partial x}) \qquad (2)$$

$$S^v=\frac{\partial}{\partial x}(\mu \frac{\partial u}{\partial r})+\frac{1}{r}\frac{\partial}{\partial r}(r \mu \frac{\partial v}{\partial r}) \qquad (3)$$

$$G=\mu\left\{2\left[(\frac{\partial u}{\partial x})^2+(\frac{\partial v}{\partial r})^2+(\frac{v}{r})^2\right]+\left[\frac{\partial u}{\partial r}+\frac{\partial v}{\partial x}\right]^2+\left[r\frac{\partial}{\partial r}(\frac{w}{r})\right]^2+\left[\frac{\partial w}{\partial x}\right]^2\right\} \qquad (4)$$

where u , v and w are the axial, radial and tangential velocities, respectively. ϕ is the general dependent variable. x and r are the axial and radial coordinates. ρ and Γ_ϕ are the density and the effective diffusivity coefficients. S_ϕ is the source of ϕ . In the present calculations, equations were solved for mean continuity and with dependent variables, ϕ , corresponding to the axial, radial and tangential velocity components. The effective diffusivity was calculated from the two-equations k- ε turbulence model.

Table 1. The form of the source terms in the general equation (Eq. (1))

ϕ	Γ_ϕ	S_ϕ
1	0	0
u	μ	$-\frac{\partial p}{\partial x}+S^u$
v	μ	$-\frac{\partial p}{\partial r}+\frac{\rho w^2}{r}-\frac{2\mu v}{r^2}+S^v$
w	μ	$-\frac{\rho v w}{r}-\frac{w}{r^2}\frac{\partial}{\partial r}(r\mu)$
k	μ/σ_k	$G-C_D \rho \varepsilon$
ε	μ/σ_ε	$(C_1 G \varepsilon - C_2 \rho \varepsilon^2)/k$

The effective viscosity, μ, and the length scale of turbulence motion, ℓ, are given by the following equations, respectively.

$$\mu = \mu_\ell + \rho C_\mu k^2 / \varepsilon \tag{5}$$

$$\ell = C_\mu k^{3/2} / \varepsilon \tag{6}$$

where μ_ℓ is the laminar viscosity. The standard k-ε turbulence closure model involves five modeling constants, summarized in table (2). These values are recommended by Launder and Spalding [8] based on extensive examination of turbulent flows.

Table 2. Empirical constant in k-ε model

C_μ	C_1	C_2	σ_k	σ_ε
0.09	1.44	1.92	1.0	1.3

2-2 Boundary Conditions and Solution Procedure

The domain over which the equations have to be integrated is that enclosed by the inlet and outlet sections, the axis of symmetry and the solid wall, as shown in Fig. (1). The inlet boundary conditions were taken from the measurements where possible. The distribution of the turbulence kinetic energy, k, at the inlet was assumed uniform and the value was estimated using a fixed turbulence intensity when experimental values were not available. The rate of energy dissipation, ε, at the inlet section was not available for all tested cases and the value was estimated using a fixed length scale at the inlet with the following expression,

$$\varepsilon_{in} = C_\mu k^{3/2} / \ell \tag{7}$$

where ℓ is the characteristic length scale of turbulence, equation (6). At the exit plane, all of the streamwise gradients of unknown variables were presumed to be constant and overall mass conservation through each cross section was imposed. The wall function was used to reduce the number of grid points near the wall. At nodes nearest to the solid walls, the velocity vector is assumed to be on the plane parallel to the solid walls and local equilibrium is assumed for the turbulence quantities. On the solid wall, the no-slip velocity boundary condition is applied. The wall shear stress, τ_w, is calculated from the log-law or its alternative form,

$$\tau_w = \rho C_\mu^{1/4} k_p^{1/2} \aleph V_p \tag{8}$$

in which subscript, p, refers to the adjacent node to the wall, $\aleph$ is von' Karman's constant and V_p is the velocity parallel to the wall under consideration. The rate of energy dissipation at this node is obtained from the following expression,

$$\varepsilon_p = C_\mu^{3/4} k_p^{3/2} / \aleph y_p \tag{9}$$

where y_p is the distance from the wall and $\aleph = 2.4$

A staggered grid system is employed in the present computation so that the grid lines do not coincide with the diffuser wall. In this method, the diffuser wall surface must be approximated by step-like surfaces, as shown in Fig. (2). The discretization of the governing equations are obtained by integrating the differential equations over a finite control volumes. The system of equations with the preceding boundary conditions are solved by a finite difference technique. Central differencing is used for diffusion terms while hybrid differencing is used for the convective terms [19]; source terms were linearized. The solution procedure is based upon the SIMPLE algorithm. A complete description of the solution procedure was found in Ref. [20]. The numerical solution was obtained when the relative residuals of the total mass flow rate and velocities are less than 0.001.

3- RESULTS AND DISCUSSIONS

In this section, selected numerical predictions are presented and compared with the available measurements for two sets of experimental data on the diffuser flow with the effects of the inlet swirl and the inlet turbulence intensity.

3-1 Effects of Inlet Turbulence Intensity

Various experimental studies have indicated that certain types of separation and transitory stall in diffusers can be avoided by changing the inlet flow conditions. The experimental data of Sajben et. al. [7] were used to examine the effect of inlet turbulence intensity and inlet velocity profile on the performance of conical diffusers. The configuration is a conical diffuser with a total expansion angle of 12 degrees and area ratio of 2.43. To alter the inlet flow conditions, thin screens with non-uniform solidity were placed upstream the inlet section of the diffuser. The tested inlet conditions are summarized in the following table (3),

Table 3. Inlet conditions of Ref. [7]

Bin	0.059	0.068	0.103	0.164	0.244
Tu (%)	0.9	0.9	0.9	0.8	0.7

Where the inlet blockage, Bin, is defined as the ratio between the displacement thickness of the boundary layer, δ^*, to the diffuser radius at inlet. It can be seen that increased turbulence intensity, Tu, reduces the value of inlet blockage. As mentioned in Ref. [7], all velocity profiles generated at the diffuser inlet resulted in a separated flow. They verified the existence of separation by direct observation tufts at the diffuser exit and as reflected in the measurements of the pressure recovery coefficient. Figure (3) shows the comparison of the predicted and measured diffuser performance coefficient which was defined as,

$$C_p = \frac{1/A_2 \int p_2 dA_2 - 1/A_1 \int p_1 dA_1}{\frac{1}{2}\rho (1/A_1) \int U_1^2 dA_1} \qquad (10)$$

Predictions with five values of inlet blockage and three different turbulence intensities are compared with the experimental data in Fig.(3). The comparison indicates that the calculation predicts the performance reasonably well for the different inlet conditions. The pressure recovery increases by creating a high turbulence intensity at the diffuser entrance. It is obvious also from the computation and experiments that, there is an optimum inlet turbulence intensity to obtain the maximum improvement in the diffuser performance. The predicted axial velocity profiles at diffuser exit for different inlet turbulence intensities and different inlet blockages are given in Fig. (4). The calculated exit velocity profiles confirm the experimental observation of the presence of separation at the diffuser exit. On the other hand, the separation region near the wall is shrank when the inlet flows is altered with the flow control screen. This is due to the favorable pressure gradient along the wall and the smaller blockage thus obtained. Figure (5) presents the centerline velocity along the diffuser. It can be observed that, increasing the inlet blockage, which is accompained by a reduction in turbulence level, increases the core velocity and hence reduces the pressure recovery coefficient in the diffuser. The numerical calculation predicts all of these effects clearly and can be used to provide guiding information for the advanced design.

The experimental tests of the effects of inlet turbulence intensity on the performance of a wide-angled conical diffuser is conducted by Sharan [8]. The configuration is a turbulent flow inside a conical diffuser of the total divergence angle of 15 degrees with low and high area ratios of 2.5 and 5. Tests are carried out of static pressure rise at the Reynolds number of 1×10^5 for three different inlet turbulence levels. The turbulence intensity level of the inlet flow is indicated by the core turbulence intensity. Potential core turbulence intensity for the naturally developing flow was of the order of 1.05% and for flow with fixed transition was 4.6% and 8.1%. Wire gauzes were used as turbulence generators to produce high intensity turbulence at the diffuser inlet.

A comparison between the measured and predicted overall pressure recovery coefficients at different free-stream turbulence intensities is shown in Fig. (6). It can be noted from this figure that, a reasonable agreement between the predicted and experimental values of the overall pressure recovery coefficients. In addition, it is noticed also that a significant improvement for the 15 degrees diffuser as the turbulence intensity increases. It can be observed from the predicted results of axial velocity at the wall and the centerline of the diffuser which are appeared in Fig. (7) to Fig. (10) that, increasing the inlet turbulence intensity has resulted in a significant increasing in the values of velocity at the wall while the velocity at the centerline is decreased. As a consequence, the separation suppressed inside the diffuser with increasing the inlet turbulence intensity due to the relaxation of the adverse pressure gradient. As shown in Fig. (11), the location of separation (X_s) moves towards the

diffuser exit as the turbulence intensity increases. This is true and more pronounced in the diffuser with low area ratio, AR = 2.5.

Although a lot of experimental work has been carried out on conical diffusers, few of them provide detailed measurements of nonseparating flow inside the diffuser, particularly in the near-wall region. Also, the effect of turbulence intensity on the performance of non-separating flow inside the diffuser is not examined. Trupp et. al. [21] conducted detailed near-wall measurements of the flow in a conical diffuser. This data set is most suitable for validating the present computation. The analysis also includes an examination of the effect of turbulence intensity on the diffuser performance. In Ref. [21], the measurements were obtained in a conical diffuser having a total divergence angle of 8 degrees and an expansion area ratio of 4. The calculations are carried out for Re = 1.15×10^5 and the inlet conditions were obtained from the measurements. The turbulence kinetic energy profile was assumed to be the same as that of fully developed flow. The dissipation rate of turbulence kinetic energy at the inlet is approximated by,

$$\varepsilon_{in} = k^{3/2} / \ell \qquad (11)$$

based on the equilibrium assumption and the data in Ref. [22].Where ℓ is the characteristic mixing length and is taken of 0.2 of the inlet radius of the diffuser. The predicted and measured developments of the axial velocity profiles are given in Fig. (12), while the predicted developments of the turbulence kinetic energy profile are shown in Fig. (13). The comparison between the calculated and measured pressure recovery coefficient along the diffuser wall and for the centerline velocity are shown in Fig.(14) and Fig. (15), respectively. It can be seen from the comparison that, the agreement between the present calculations and the measurements is excellent. Unfortunately, the effect of turbulence intensity on the nonseparating flow in conical diffusers is not clarified. As shown in Fig. (13), a peak in the turbulence kinetic energy profile is noticed at the wall region and then shifted towards the diffuser centerline as the flow moves in the downstream direction.

In the previous investigations, it is observed that, as the turbulence level in the free stream region upstream the diffuser inlet becomes higher, the diffuser performance was improved. However, it is impossible to find out which local turbulence in the free stream or near the wall influences the diffuser performance. The object of the present calculations is to establish the nature of the dependence of the overall diffuser performance on inlet turbulence level and correspondingly on the inlet velocity profile.

Calculations are performed to study the behavior of flow inside 8 and 20 degrees conical diffusers with area ratios of 4 and 6, respectively. The artificial method used to generate increased levels of inlet turbulence, namely thin annular rings located upstream of the diffuser, Fig. (1). It was resulted that the presence of rings would change the turbulence pattern and velocity profile of the flow at the diffuser entrance. For 8 degrees diffuser, the computations are performed at Re = 1.15×10^5 for uniform inlet flow conditions while the

Reynolds number, Re, is taken 68000 in the case of 20 degrees diffuser. To alter the inlet flow conditions, rings with different porosity are used, namely the porosity, ψ, was taken as 0.5, 0.7 and 0.85. Porosity equal one denotes flow through diffusers without rings. The developments of the diffuser performance with and without the flow control rings are compared. The calculated velocity profiles and turbulence kinetic energy distributions at the diffusers entrances are given in Fig. (16) and Fig. (17), for different porosities. It can be observed from these figures that, the non-uniformity of the inlet velocity profile increases with decreasing the ring porosity while the turbulence level is increased. It was found that the free stream turbulence intensity increased from 2.7% to 7.0% in the presence of rings. Correspondingly, the overall pressure recovery of 8 degrees diffuser is increased by 5.7% and by 31.5% with the 20 degrees diffuser, as shown in Fig. (18) and Fig. (19), respectively. It can be observed also that the initial stages of 8 degrees diffuser are sensitive to the inlet conditions while the final stages of it are less sensitive to the initial conditions, as shown in Fig. (18). On the other hand, the wide-angled diffuser, 20 degrees, is strongly affected by the inlet conditions due to the rapid change of the turbulent flow inside it, as shown in Fig. (19). It can also be seen from Fig. (20) and Fig. (21) that, the exit velocity profiles with upstream rings are symmetrical and uniform while the exit velocity profiles without upstream rings are highly distorted. In addition, the separation tendency in 20 degrees diffuser disappeared with increasing the turbulence intensity. The significant improvement in the velocity profiles for the conditions of the upstream rings is attributed to improved turbulent mixing, where the eddies generated by the upstream rings effectively transmit free stream energy to the diffuser wall. Therefore, it appeared from the computational results that the local turbulence level in the wall region strongly affects the diffuser performance. This was explained also by Hoffmann [16]. The improvement in values of the pressure recovery is a result of the improved velocity profile with reduced distortion and delayed separation. It can be concluded also that, the effect of inlet turbulence pattern on overall performance for non-separating flow in small-angled diffuser is expected to be relatively small while the turbulence pattern at the entrance of the wide-angled diffuser influences the occurrence of separation.

3.2 Effects of Inlet Swirl Intensity

The experimental data of Neve and Wirasinghe [11] are used for comparison purposes. The measurements were conducted with five different conical diffusers of total divergence angles of 10, 15, 20, 25 and 30 degrees to clarify the influence of swirl on the performance of conical diffusers. The Reynolds number at the diffuser inlet was up to 46600. Three swirl intensities equivalent to swirl angles of 8.6, 10.9 and 15 degrees were tested for each diffuser configuration. The measured swirl velocity profile at the inlet is a linear function of radius over 90% of the radius and the swirl is the solid-vortex type. The measured profiles of axial and tangential velocity components at the diffuser inlet are used for the calculations. The variations of local pressure recovery coefficients, Cp, along the 30 degrees diffuser for swirling and non-swirling flow are shown in Fig. (22). The predictions are in good agreement

with the experimental data of 30 degrees diffusers. For a swirl angle of 15 degrees, the computation give slightly larger values than those measured. The effect of swirl on the overall pressure recovery coefficient, Cp_0, for all tested diffusers in Ref. [11] is shown in Fig. (23). The flows with additional amounts of swirl are also numerically simulated and the predicted results are compared for all tested diffusers. The results indicate that the addition of a swirl to an axial flow in a conical diffuser can lead to improvements in static pressure recovery and hence in efficiency. This conclusion apply to conical diffusers having moderately or hardly separated axial flow. On the other hand, swirling inlet flow slightly affects the performance of diffusers which having unseparated axial flow, as shown for 10 degrees diffuser in Fig. (23). This may be attributed to the increase of frictional losses inside the diffuser.

Unfortunately, the experimental results did not pursue the optimum swirl angle or optimum swirl intensity required to obtain the maximum pressure recovery coefficient or maximum efficiency of tested diffusers. Therefore, a computational study is performed to find out the optimum swirl intensity of conical diffusers with included angles ranged from 10 to 30 degrees. Figure (24) presents the results of the overall pressure recovery coefficient with additional amount of swirl up to an inlet swirl angle of 45 degrees. The predicted results indicate that the optimum swirl angle for the diffuser configuration with total included angle larger than 10 degrees is ranged from 30 to 35 degrees. On the other hand, swirl angle between 10 to 15 degrees is required for small-angled diffusers to get an optimum pressure recovery coefficient. The main reasons for existing an optimum swirl intensity is that, with the swirling inlet flow, the flow inside the diffuser is pressed towards the wall and the boundary layer development and the flow separation along the diffuser wall is suppressed as shown in Fig. (25). This effect enhances the turbulent mixing near the wall, as presented in Fig. (26), and decreases the boundary layer thickness. As a consequence, the pressure recovery increases due to the reduction of turbulent flow losses. However, the strong swirl also creates a very low small velocity or reversed velocity region near the centerline which increase the turbulent flow losses and the effective area is decreased and results in a low pressure recovery coefficient. As shown in Fig. (27), the numerical prediction indicates that there exists a recirculated flow region near the centerline of the 30 degrees diffuser when the swirl intensity is high, namely, the swirl angle is equal to 45 degrees. Hence, the maximum efficiency of the diffuser is obtained by trading of the effects between boundary layer thickness and the effective flow area brought about by swirl.

An extended computational study is conducted to determine the effect of swirling inlet flow on the performance of conical diffusers with unseparated and fully separated axial flow. For this purpose, seven different conical diffusers were tested theoretically with total divergence angles ranging from 10 to 70 degrees and with area ratio of 4. The calculated overall pressure recovery for different swirl angle is illustrated in Fig.(28). It can be seen from this figure that, swirling inlet flow slightly affects the performance of small-angled diffusers which having unseparated axial flow. For wide-angled diffusers which

are moderately or fully separated for axial inlet flow, swirling inlet flow caused large performance improvements based on swirl intensity. For example, detailed predictions of flow characteristics in 30 degrees diffuser are reported at different sections and for different inlet swirl intensities. The distribution of the swirl velocity component at the inlet section is very similar to that of the solid-body vortex type of swirl. The flow parameters are plotted at X/Ld = 0.2, 0.4, 0.6, 0.8 and 1.0 and the swirl angle is varied from 0.0 to 45 degrees. The predicted developments of the axial velocity profile are given in Fig. (29). The developments of the predicted swirl velocity profiles are shown in Fig. (30). The ail velocity profiles indicate that there exists a separation near the diffuser wall at X/Ld = 0.2 up to the diffuser exit with the non-swirling flow. The wall separation region is suppressed and completely eliminated when the swirl angle becomes 45 degrees. This is attributed to the increase of angular momentum in the diffusers as shown in Fig. (30). However, the strong swirl also creates a reversed velocity region near the diffuser centerline. This can be explained as follows : as shown from the swirl velocity profiles, with the strong swirl, a large solid vortex core is developed at the core region and a low pressure region is created near the centerline, as illustrated in Fig. (31). When the difference between the wall static pressure and the centerline static pressure becomes greater than the dynamic pressure of the axial flow, a stagnation or back flow region is formed at the centerline. Harvey [23] and So [24] also observed experimentally the recirculated or reversed region near the centerline when the flow has a strong swirl. Unfortunately, So did not give the swirl conditions at the point when the reverse flow first appeared. In the present study, the swirl angle at which the reverse flow starts in the core region inside the diffuser will discussed below with the discussion of the decay of swirl.

The distributions of turbulence intensity at different locations inside the 30 degrees diffuser for different swirl angles are shown in Fig. (32). It can be observed that, the maximum turbulence intensity moves towards the wall with increasing the swirl which leads the increase of the centrifugal force. Clearer evidence of the increase mixing at the diffuser wall due to increasing swirl is given by the reduction in boundary layer thickness as can be observed in Fig. (29). The increased mixing increases the turbulence level and acts like an effective increase in Reynolds number.

The effects of flow regimes in conical diffusers on the decay of swirl are predicted. As an example, the axial and swirl velocity distributions at many sections inside the conical diffusers with divergence angles of 4, 8, 40 and 70 degrees are presented in Fig. (33) to Fig. (36), for a swirl angle of 30 degrees. For unseparated flow regime, Fig. (33) and Fig. (34), the swirl velocity profiles indicate that the flow behaves either like a solid-body rotation over 90% of the radius. The decay of swirl in small-angled conical diffusers is indicated by the gradual downstream decreases of the slope of the swirl velocity. This means that the swirl decay in small-angled conical diffusers is approximately similar to that in pipes. On the other hand, as shown from Fig. (35) and Fig. (36), the slope of swirl velocity profiles increases for diffusers which are moderately or badly separated for axial inlet flow. Consequently, the swirl angles increase in

the wide-angled conical diffusers due to the presence of separation. Therefore, it can be concluded that, the decay of swirl in conical diffusers is strongly affected by the flow regimes. The swirl condition at which the reverse flow in the core region inside the conical diffuser with the divergence angle of 30 degrees is predicted. Since the swirl angle increase in separated conical diffuser, the reverse flow should first appears at the diffuser exit. The predicted results of axial and tangential velocity profiles which are shown in Fig. (37) indicate clearly that, the reverse flow near the centerline appears at the diffuser exit when the swirl angle is equal to 37 degrees. It can be also noticed from this figure that, the flow reattachment to the diffuser wall at the exit is observed. At this swirl condition, $\beta = 37$ degrees, the decay of swirl is started and the diffuser yielded the maximum overall pressure recovery coefficient as indicated in Fig. (38). Further increase in swirl angle causes a reduction in the overall pressure recovery coefficient. In summary, the optimum swirl angle which is required to obtain the maximum improvement in the diffuser performance can be defined as the angle which gives swirl intensity to remove the separation tendency at the wall and not enough to induce a reverse flow in the core region.

4- CONCLUSIONS

The numerical prediction of the turbulent flow filed in the conical diffusers with the k-ε model of turbulence is studied. The numerical calculation is based on the fully conservative control volume representation of the governing conservation equations. Complex turbulent flows inside various conical diffusers with the effects of inlet turbulence intensity and inlet swirl are numerically predicted. The important conclusions drawn from this study are:

1- The numerical prediction of the complex turbulent flows inside conical diffusers under the effects of the inlet turbulence and the inlet swirl compares generally well with the experiments. The numerical calculations provide a useful guidance for the design purpose.

2- The effect of increasing inlet turbulence is to improve the diffuser performance. The overall pressure recovery of 8 degrees diffuser is increased by 5.7%. The percentage increase becomes 31.5% with 20 degrees diffuser, when the inlet free-stream turbulence increased from 2.7% to 7% in both diffusers. An optimum inlet turbulence intensity for improving the diffuser performance is observed.

3- Swirl can be used to improve the diffuser performance, especially in wide-angled diffusers based on the inlet swirl intensity. The wall separation in such units is suppressed and completely eliminated with increasing the swirl intensity. However, the strong swirl creates a reversed velocity region near the diffuser centerline.

4- An optimum value of swirl is found which give maximum performance. The maximum performance is determined by trading of the effects between boundary layer thickness and effective flow area brought about by swirl.

5- The swirl decay is strongly affected by the flow regimes in the conical diffusers. For unseparated conical diffusers, the decay of swirl is similar to that in pipes while the swirl angles increased in separated conical diffusers.

REFERENCES

1- Winternitz, F. A. L., and Ramsay, W. J., "Effects of Inlet Boundary Layer on Pressure Recovery, Energy Conversion and Losses in Conical Diffusers," Journal of The Royal Aeronautical Society, Vol. 61, No. 2, 1957, p. 116.

2- Cockrel, D. J., and Markland, E.,"The Effects of Inlet Conditions on Incompressible Fluid Flow through Conical Diffusers," Journal of The Royal Aeronautical Society, London, England, Jan. 1962, p. 51.

3- Bradshaw, P., "Performance of A Diffuser with A Fully Developed Pipe Flow at Entry," Journal of The Royal Aeronautical Society, 1963, p. 733.

4- McDonald, A. T., and Fox, R. W., "An Experimental Investigation of Incompressible Flow in Conical Diffuser," Int. Journal of Mechanical Science, Vol. 8, No. 2, 1966, p. 125.

5- Sovran, G., and Klomp, E. D., "Experimentally Determined Optimum Geometries for Rectilinear Diffuser with Rectangular Conical and Annular Cross-section," Fluid Mechanics of Internal Flow, American Elsevier Publishing Co., Inc., New York, N. Y., 1967.

6- Klein, A., "Review : Effects of Inlet Conditions on Conical Diffusers Performance," Trans. ASME, Journal of Fluids Engineering, Vol. 103, June 1981, p 250.

7- Sajben, M., Kroutil, J. C., and Sedrick, A. V., "Conical Diffuser Flows with Natural and Screen-Simulated Inlet Conditions," AIAA Journal, Vol. 14, No. 12, 1976, p. 1723.

8- Sharan, V. K., "Improving Diffuser Performance by Artificial Means," AIAA Journal, Vol. 10, No. 8, 1972, p. 1105.

9- McDonald, A. T., Fox, R. W., and Van Dewoestine, R. V., "Effects of Swirling Inlet Flow on Pressure Recovery in Conical Diffusers," AIAA Journal, Vol. 6, No. 10, 1971, p. 2014.

10- Senoo, Y., Kawaguchi, N., and Nagata, T., "Swirl Flow in Conical Diffusers," Bulletin of JSME, Vol. 21, No. 151, 1978, p. 112.

11- Neve, R. S. and Wirasinghe, N. E. A., "Changes in Conical Diffuser Performance by Swirl Addition," Journal of Aeronautical Quarterly, Aug. 1978, p. 131.

12- Armfield - Steven, W., Cho - Nam - Hyo. and Fletcher - Clive, A. J., "Prediction of Turbulence Quantities For Swirling Flow in Conical Diffusers,"AIAAJournal,Vol.28, No. 3, Mar. 1990, p. 453.

13- Clausen, P. D., Koh, S. G., and Wood, D. H., "Measurements of A Swirling Turbulent Boundary Layer Development in A Conical Diffuser," Experimental Thermal and Fluid Science, Vol. 6, No. 2, Jan. 1993, p. 39.

14- Moore, C. A., and Kline, S. J., "Some Effects of Vanes and Turbulence on Two-Dimensional Wide-Angle Subsonic Diffusers," Department of Mechanical Engineering, Stanford University, Sept.,1955.

15- Sajben, M., Chen, C. P., and Kroutel, J. C., "A New Passive Boundary Layer Control Device," Journal of Aircraft, Vol. 14, No. 7, Jully 1977, p. 654.

16- Hoffmann, J. A., "Effects of Free-Stream Turbulence on Diffuser Performance," Trans. ASME, Journal of Fluids Engineering, Vol. 103, Sept. 1981, p. 385.
17- Lilley, D. G., "Primitive Pressure-Velocity Code for the Computation of Strongly Swirling Flows," AIAA Journal, Vol. 14, June 1976, p.749.
18- Launder, B. E., and Spalding, D. B., "The Numerical Computation of Turbulent Flows," Methods in Appl. Mech. Engg., Vol. 3, 1974, p. 269.
19- Pantankar, S. V., "Numerical Heat Transfer and Fluid Flow," Hemisphere - McGraw-Hill, New York, 1980.
20- Gosman, A. D., and Pun, W. M., "Calculation of Recirculating Flows," Rept. No. HTS/74/12, 1974, Dept. of Mechanical Engineering, Imperial College, London, England.
21- Trupp, A. C., Azad, R. S., and Kassab, S. Z., "Near Wall Velocity Distribution within A Straight Conical Diffuser," Experiments in Fluids, Vol. 4, No. 8, 1986, p. 319.
22- Lai, Y. G. , So, M. C., and Hwang, B. C.,"Calculation of Planar and Conical Diffuser Flows," AIAA Journal, Vol. 27, No. 5, 1989, p. 542.
23- Harvey, J. K., "Some Observations of the Vortex Breakdown Phenomenon," Journal of Fluid Mechanics, Vol. 14, Pt. 4, Dec. 1962, p. 585.
24- So, Kwan L., "Vortex Phenomena in Conical Diffuser," AIAA Journal, Vol. 5, No. 6, June 1967, p. 1072.

NOMENCLATURE

A	cross-sectional area
AR	diffuser area ratio, A_2 / A_1
B	blockage factor, $2\delta^* / R$
Cp	pressure recovery coefficient, $C_p = (p - p_{in}) / 0.5\,\rho\, U_{in}^2$
p	static pressure
R	diffuser radius at a given section
Tu	turbulence intensity in the axial direction, k / U_{in}^2
U	average axial velocity at diffuser inlet
ψ	porosity, the ratio between the opening diameter of the ring to the diffuser diameter at inlet.

Subscripts

1, 2	inlet and exit stations, respectively
cl	centerline
in	inlet
w	wall

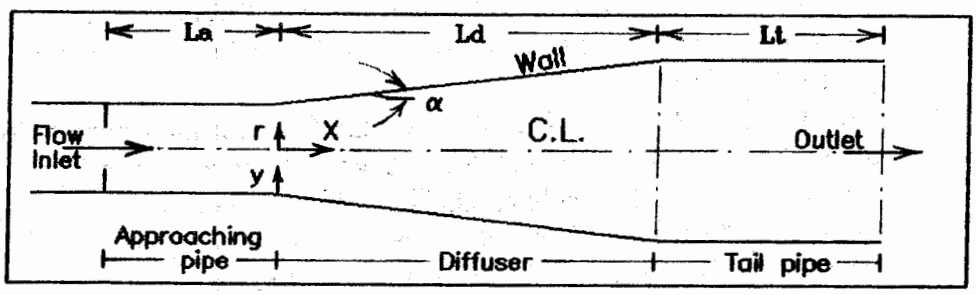

Fig. 1. Geometry of conical diffuser with approaching pipe and tail pipe.

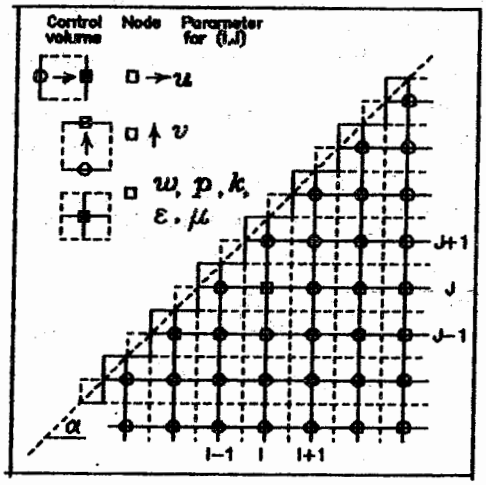

Fig. 2. Staggered grid and control volume for all flow parameters.

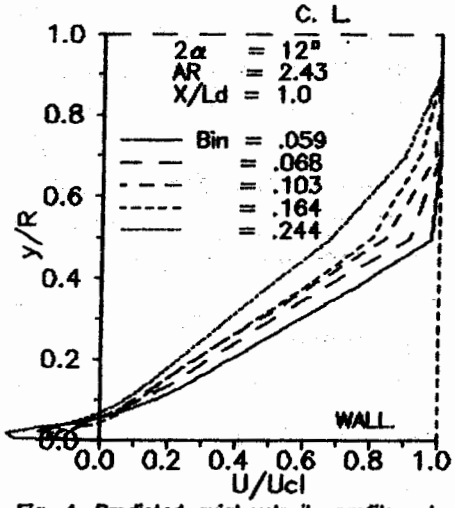

Fig. 4. Predicted axial velocity profiles at exit for different inlet boickage, Ref.[7].

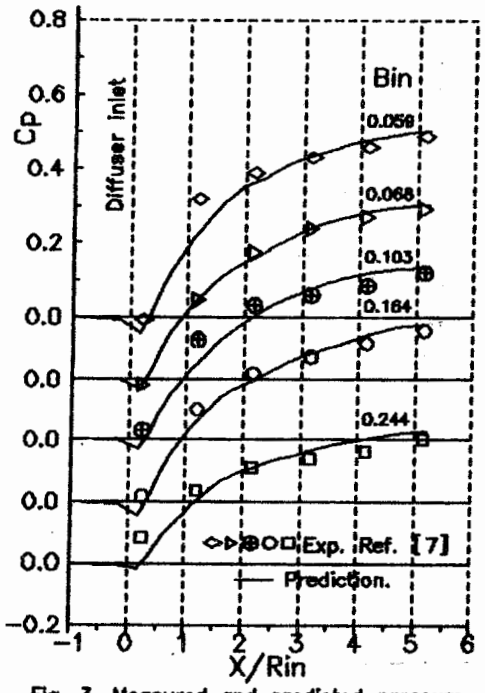

Fig. 3. Measured and predicted pressure recovery coefficients at different inlet blockage.

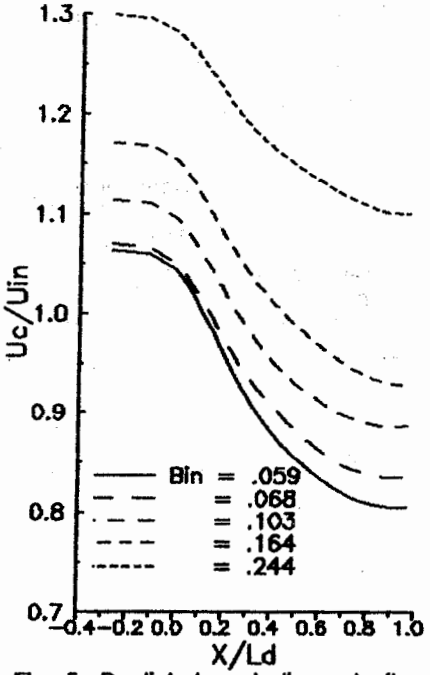

Fig. 5. Predicted centerline velocity distributions along the conical diffuser, Ref.[7].

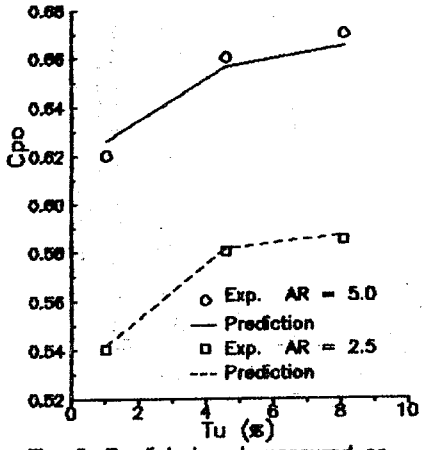

Fig. 6. Predicted and measured pressure recovery coefficient, Ref.[8].

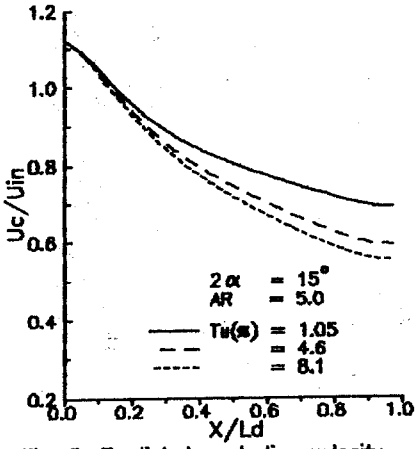

Fig. 9. Predicted centerline velocity distributions along the conical diffuser.

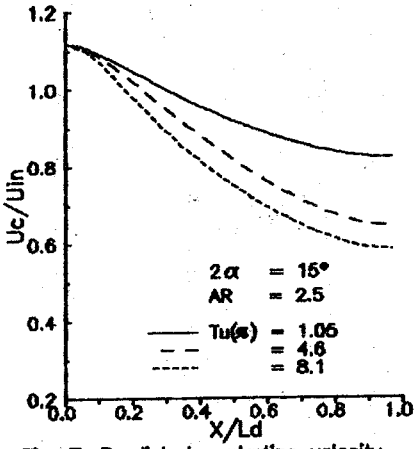

Fig. 7. Predicted centerline velocity distributions along the conical diffuser.

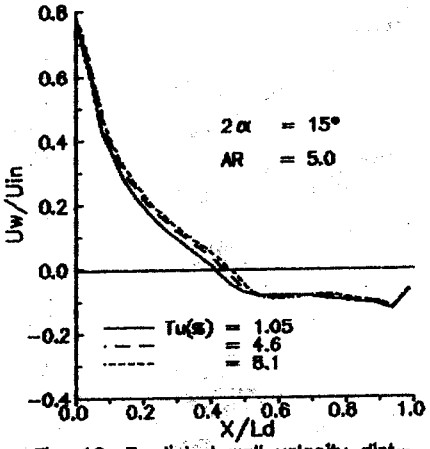

Fig. 10. Predicted wall velocity distributions along the conical diffuser.

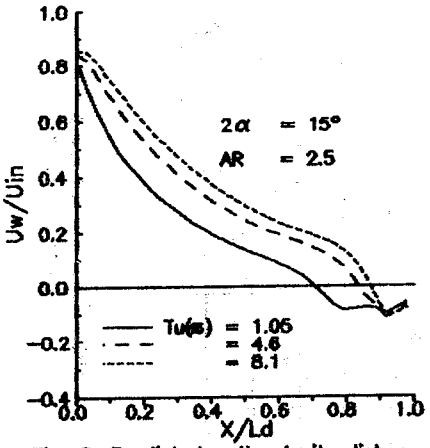

Fig. 8. Predicted wall velocity distributions along the conical diffuser.

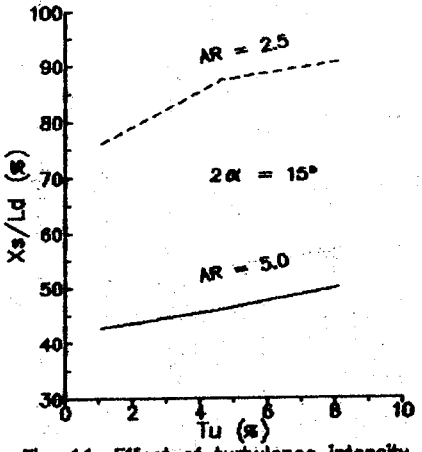

Fig. 11. Effect of turbulence intensity on separation location.

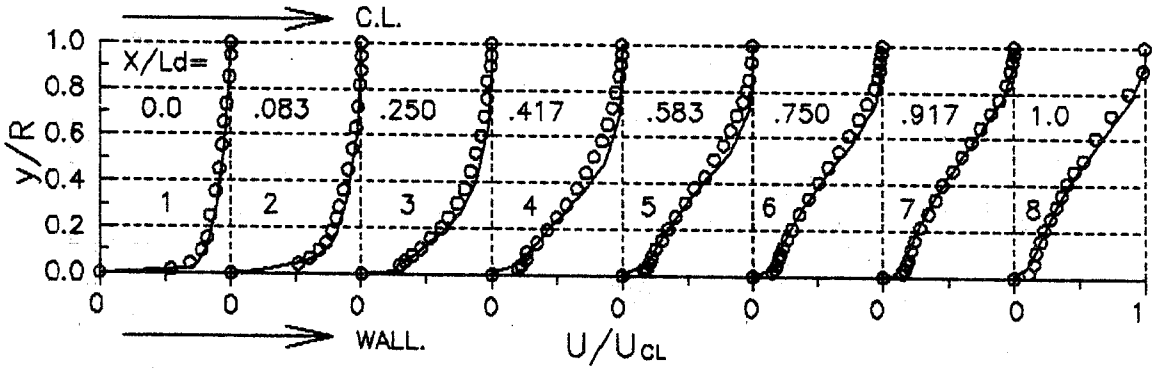

Fig. 12. Comparison between predicted and measured axial velocity profiles at different cross-sections, Ref.[21].

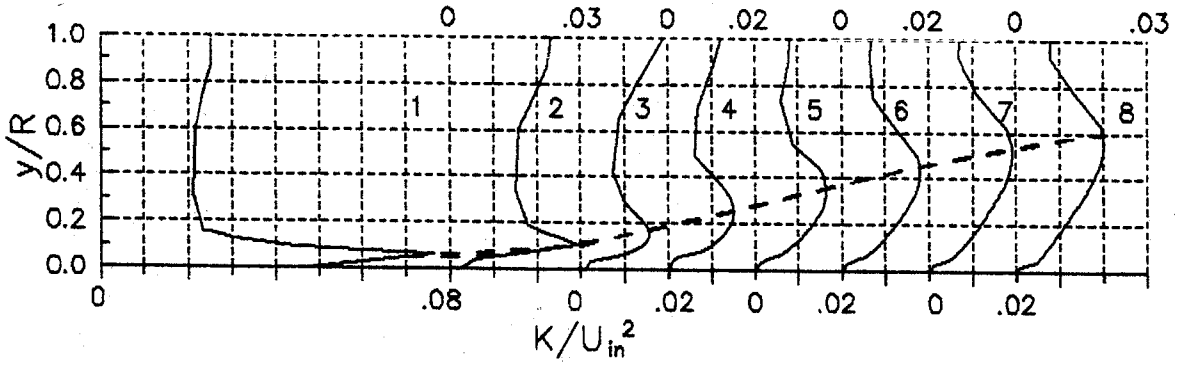

Fig. 13. Predicted turbulent kinetic energy profiles at different cross-sections corresponding to Fig. 12.

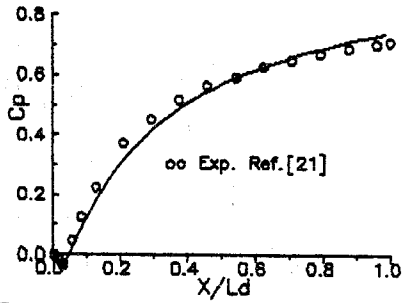

Fig. 14. Comparison between predicted and measured pressure recovery coefficient, ($2\alpha = 8°$, AR = 4.).

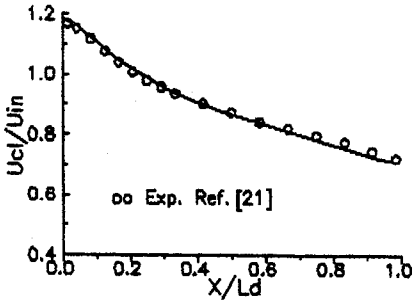

Fig. 15. Comparison between predicted and measured axial velocity along the diffuser centerline.

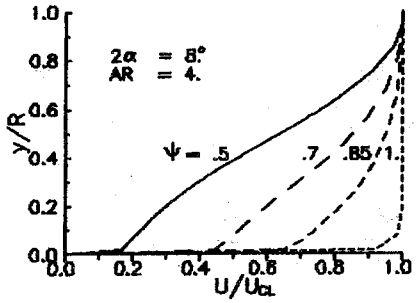

Fig. 16–A. predicted axial velocity profiles at inlet cross–section for different porosity.

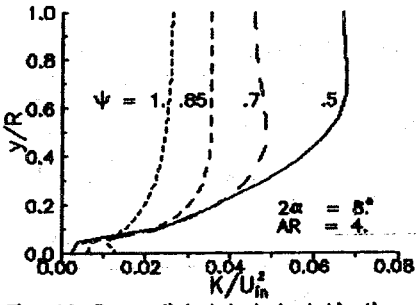

Fig. 16–B. predicted turbulent kinetic energy profiles at diffuser inlet for different porosity.

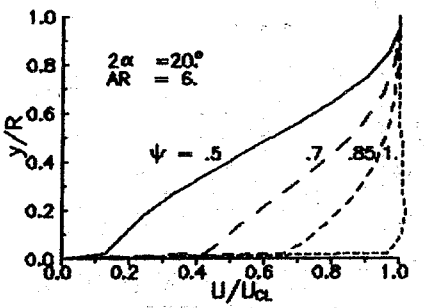

Fig. 17–A. Predicted axial velocity profiles at inlet cross–section for different porosity.

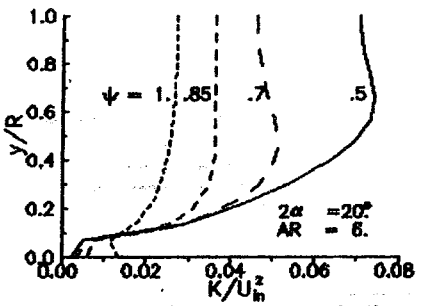

Fig. 17–B. Predicted turbulent kinetic energy profiles at diffuser inlet for different porosity.

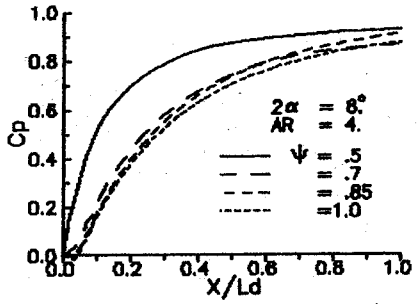

Fig. 18. Predicted pressure recovery coefficient of conical diffuser for different porosity.

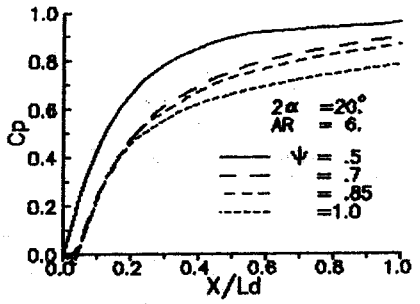

Fig. 19. Predicted pressure recovery coefficient of conical diffuser for different porosity.

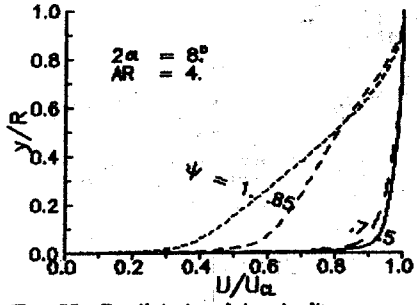

Fig. 20. Predicted axial velocity profiles at exit cross–section for different porosity.

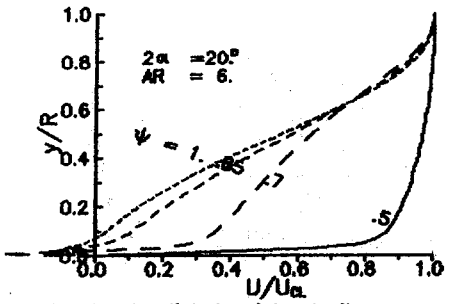

Fig. 21. Predicted axial velocity profiles at exit cross–section for different porosity.

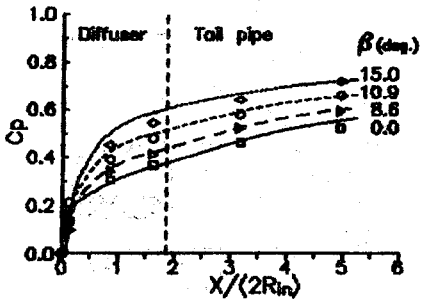

Fig. 22. Comparison between predicted and measured pressure recovery coefficient, Ref. [11].

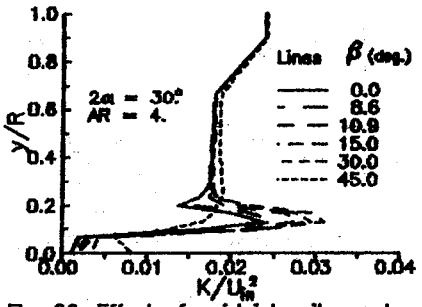

Fig. 26. Effect of swirl intensity on turbulent kinetic energy profiles at X/Ld = 0.2 .

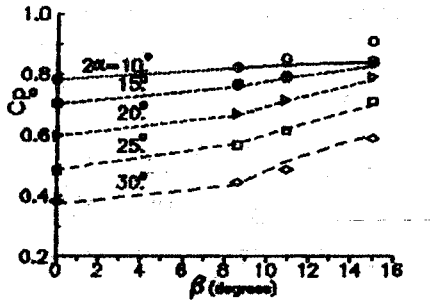

Fig. 23. Comparison between predicted and measured overall pressure recovery coefficient, Ref. [11].

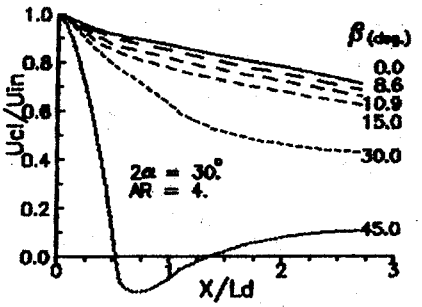

Fig. 27. Effect of swirl intensity on centerline axial velocity.

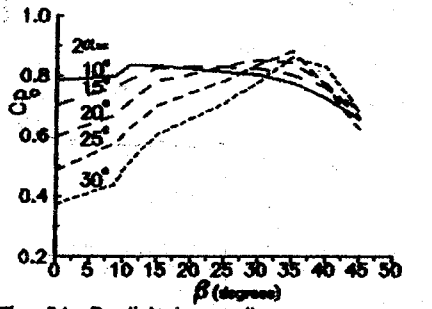

Fig. 24. Predicted overall pressure recovery coefficient at different swirl angles.

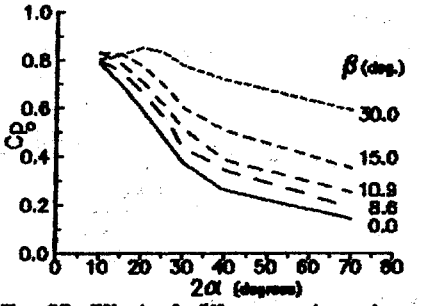

Fig. 28. Effect of diffuser angle and swirl intensity on overall pressure recovery coefficient.

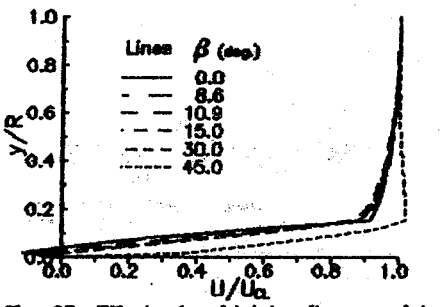

Fig. 25. Effect of swirl intensity on axial velocity profiles at X/Ld = 0.2 .

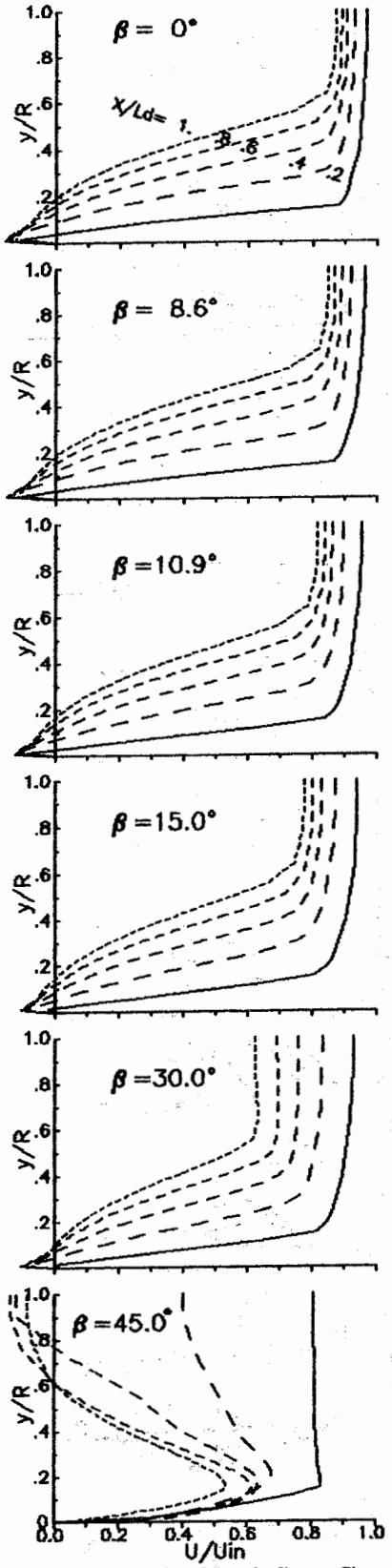

Fig. 29. Predicted axial velocity profiles at different cross-sections of conical diffuser for different swirl angles, (2α = 30°, AR = 4.).

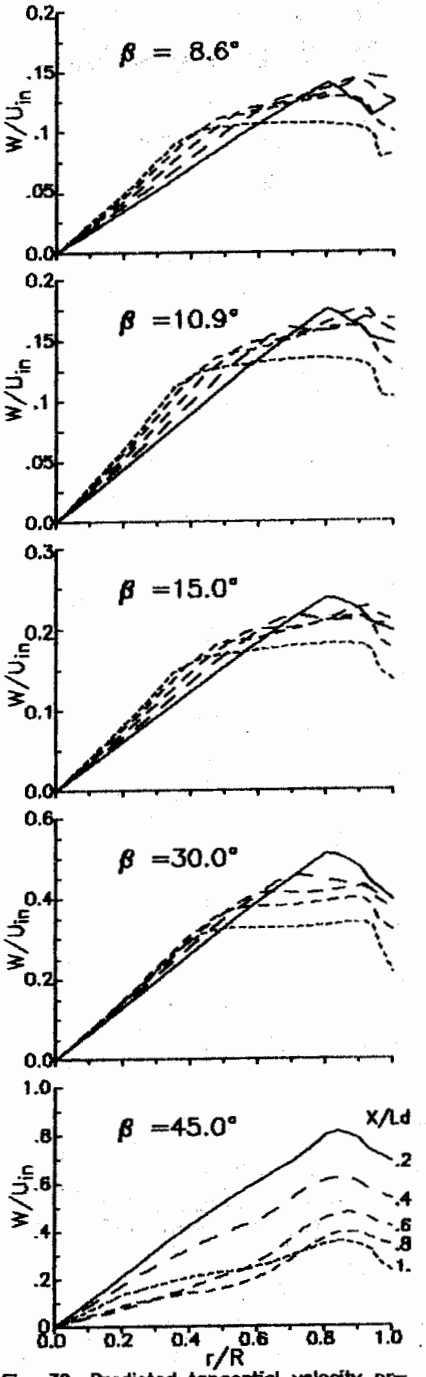

Fig. 30. Predicted tangential velocity profiles at different cross-sections with different swirl angles. (2α = 30°, AR = 4.).

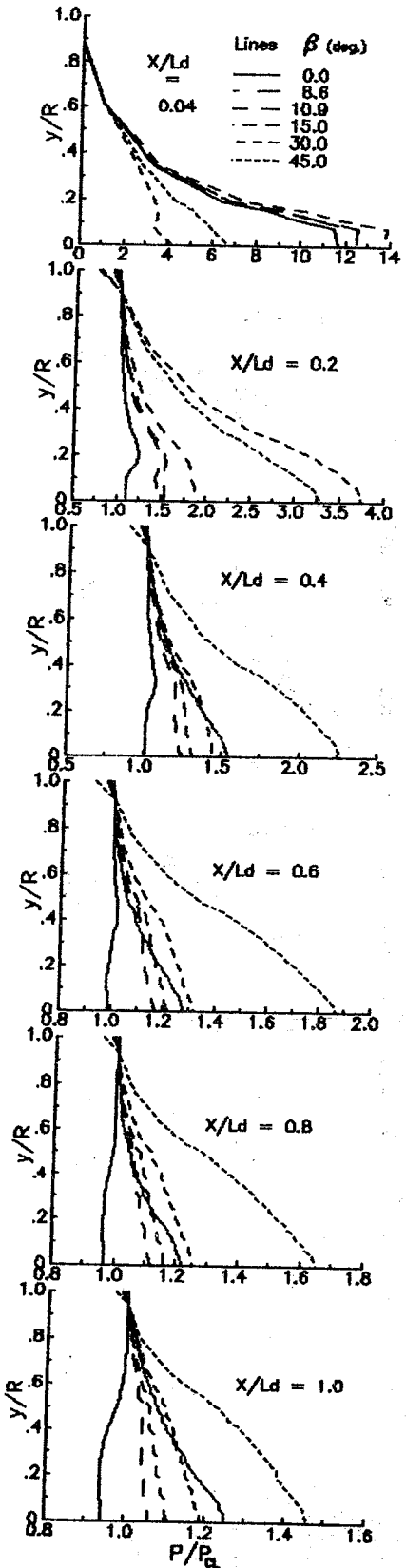

Fig. 31. Predicted pressure profiles at different cross-sections with different swirl angles for conical diffuser, (2α = 30°, AR = 4.).

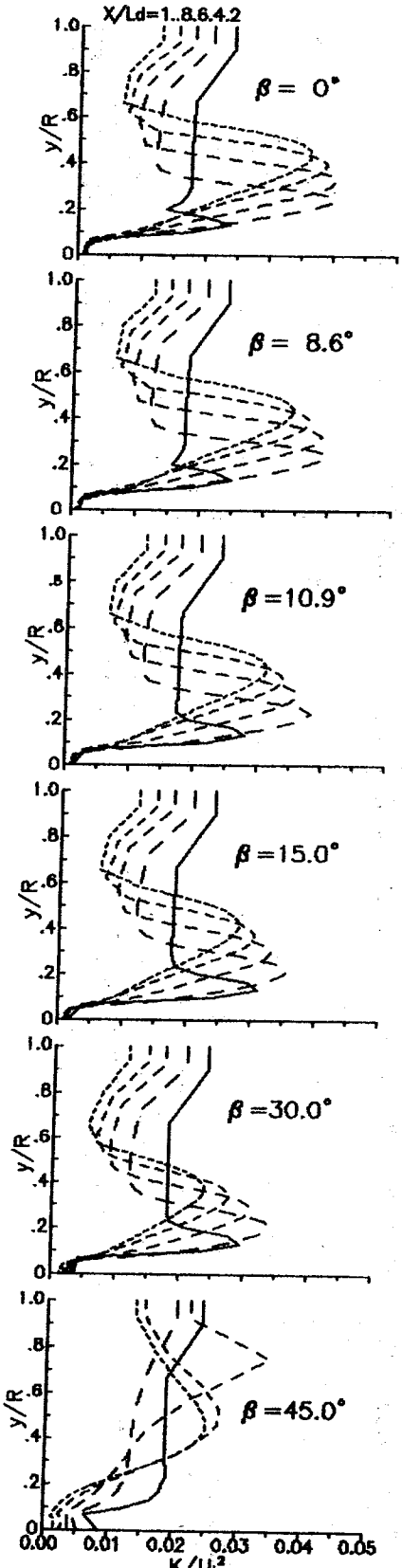

Fig. 32. Predicted turbulent kinetic energy profiles at different cross-sections with different swirl angles, (2α = 30°, AR = 4.).

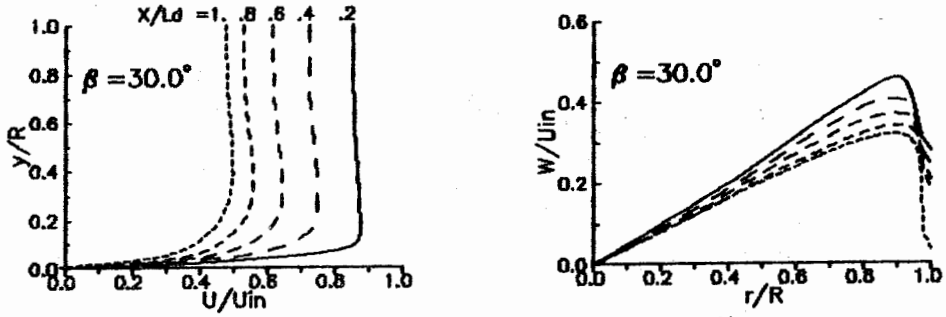

Fig. 33. Predicted axial and tangential velocity profiles for conical diffuser, (2α = 4° , AR = 2.43).

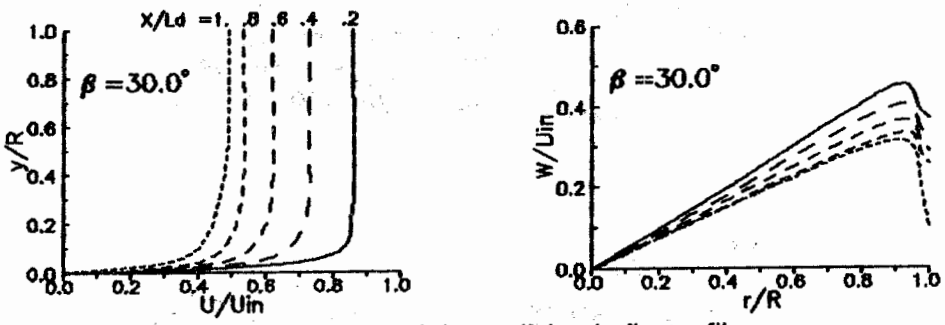

Fig. 34. Predicted axial and tangential velocity profiles for conical diffuser, (2α = 8° , AR = 2.43).

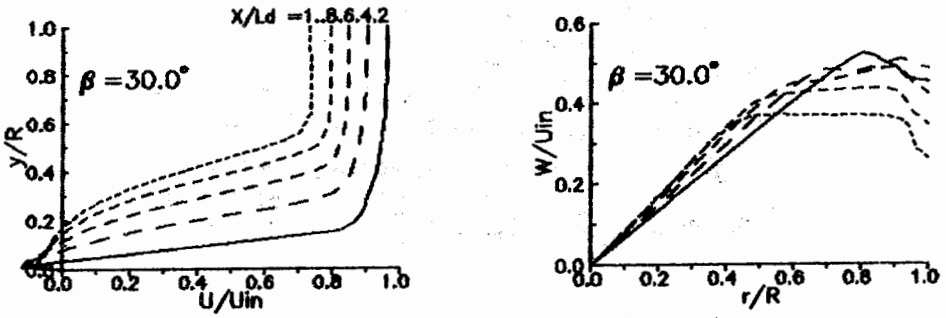

Fig. 35. Predicted axial and tangential velocity profiles for conical diffuser, (2α = 40° , AR = 4.).

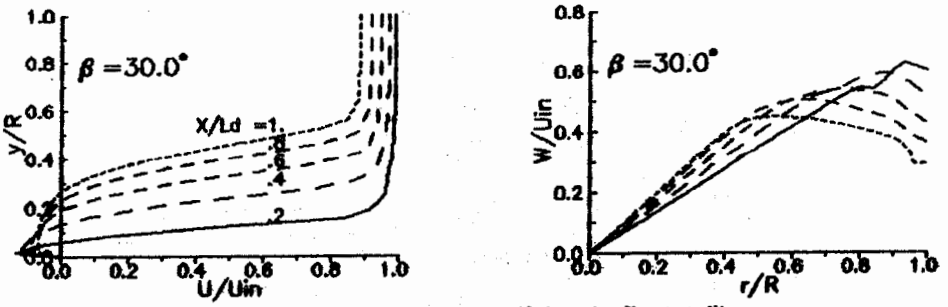

Fig. 36. Predicted axial and tangential velocity profiles for conical diffuser, (2α = 70° , AR = 4.).

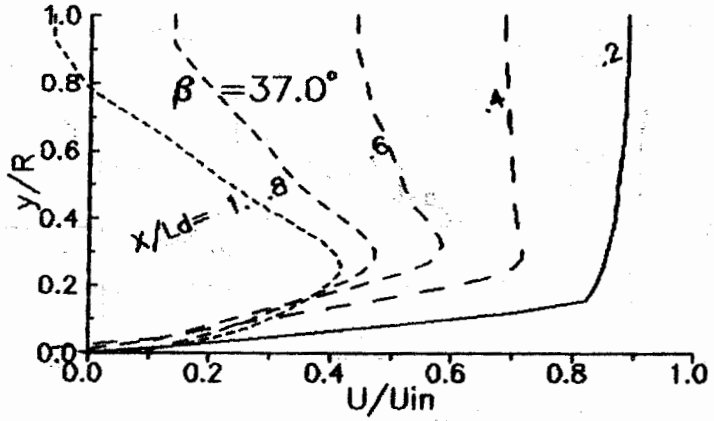

Fig. 37–A Predicted axial velocity profiles for conical diffuser, (2α =30°, AR =4.).

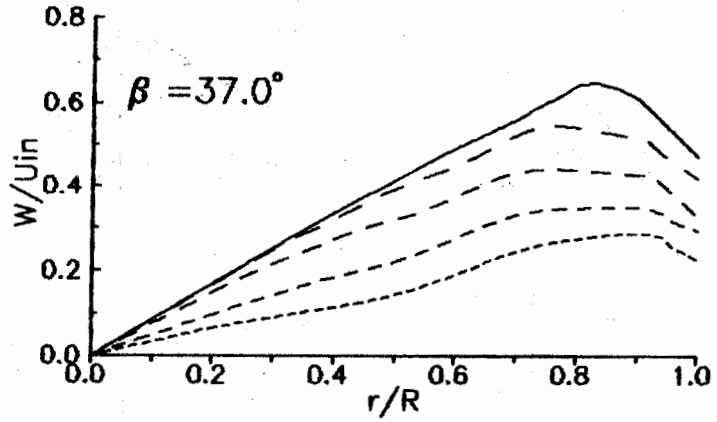

Fig. 37–B Predicted tangential velocity profiles for conical diffuser, (2α = 30°, AR = 4.).

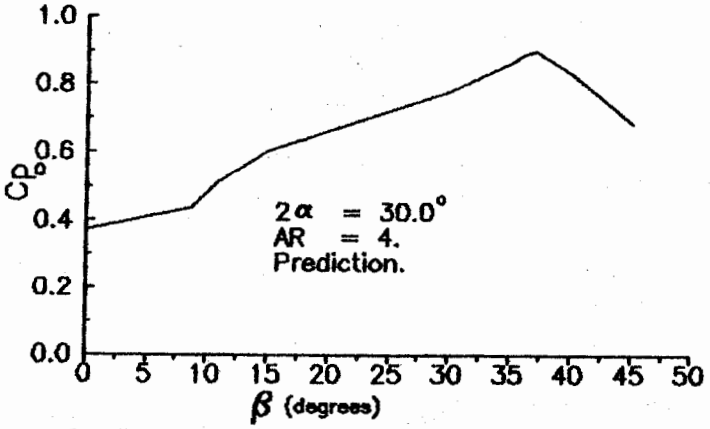

Fig. 38. Effect of swirling flow regime on the overall pressure recovery coefficient.

ملخص البحث

تأثيرات شدة الأضطرابات والدوامات عند المدخل على سريان الناشر

هذا البحث يتناول دراسة نظرية للإنسياب الإضطرابى الغير قابل للإنضغاط آخذا فى الإعتبار تأثير شدة الإضطرابات والتدويم على نمط السريان فى النواشر المخروطية ذات المقطع الدائرى. تم وضع المعادلات الحاكمة للإنسياب وهى عبارة عن معادلات كمية الحركة فى الإتجاة المحورى، القطرى، المماسى مع إستخدام النموذج الرياضى للإضطرابات للحصول على اللزوجة الإضطرابية وحساب طاقة حركة الإضطرابات فى الطبقة الجدارية بالإضافة إلى الظروف المحيطة بالسريان عند محور التماثل والجدار والمدخل والمخرج للإنسياب، كما تم توصيف الظروف الإبتدائية للسريان. وبإستخدام التحليل العددى أمكن توقع وتقييم متغيرات الإنسياب خلال النواشر المخروطية. إشتمل هذا البحث على دراسة تأثير شدة التدويم الإبتدائية كذلك تم دراسة تأثير شدة الإضطرابات عند المدخل.

أوضحت الدراسة النظرية المأخوذه من الحل الرياضى أن زيادة شدة الإضطرابات عند المدخل تؤدى إلى تحسن ملحوظ فى أداء النواشر المخروطية، كذلك بينت الدراسة النظرية وجود قيمة مثلى لشدة الإضطرابات الإبتدائية للحصول على أفضل أداء للنواشر. كما بينت الدراسة النظرية أن التدويم يؤدى إلى إختفاء ظاهرة إنفصال السريان عند الجدار وبزيادة شدة التدويم عند المدخل يؤدى إلى حدوث منطقة دوامات عند محور تماثل الناشر. كذلك أوضحت الدراسة أن وجود التدويم فى السريان خلال النواشر التى تحتوى على إنفصال للسريان يعطى تحسن كبير فى الأداء مقارنة بالنواشر التى لا تحوى إنفصال للسريان. تم إستنتاج قيمة مثلى لشدة التدويم عند المدخل التى تعطى أفضل أداء للناشر. كما تم إستنتاج أن معدل إخماد التدويم فى النواشر يعتمد على رجيم السريان. ولإختبار صحة الحل الرياضى... تم مقارنة بعض النتائج النظرية مع النتائج العملية المتاحة وقد أظهرت هذه المقارنة تقاربا معقولا بين النتائج النظرية والقياسات العملية.